Hindawi
Mathematical Problems in Engineering
Volume 2021, Article ID 5598611, 13 pages
https://doi.org/10.1155/2021/5598611

Research Article

Evaluation of Freeze-Thaw Durability of Silica Fume Concrete with Spraying Inorganic Coating Using Ultrasonic Testing

Wujian Yan,[1,2,3] **Fuhang Niu**,[3] **and Xinxin Tian**[1]

[1]*Key Laboratory of Loess Earthquake Engineering, China Earthquake Administration, 450 Donggang West Road, Lanzhou 730000, China*
[2]*Key Laboratory of Earthquake Engineering and Engineering Vibration, Institute of Engineering Mechanics, China Earthquake Administration, 29 Xuefu Road, Harbin 150080, China*
[3]*State Key Laboratory of Frozen Soil Engineering, Northwest Institute of Eco-Environment and Resources, Chinese Academy of Sciences, 382 Donggang West Road, Lanzhou 730000, China*

Correspondence should be addressed to Wujian Yan; yanwj1980@126.com

Received 7 February 2021; Accepted 20 October 2021; Published 1 December 2021

Academic Editor: Bowen Guan

To study the antifreezing durability of internal coating silicon fume concrete with different external coatings, fast freeze-thaw (FT) cycle testing was performed for three types of external coatings applied to the internal coatings of silicon fume concrete. Using ultrasonic testing and compressive strength tests, we analysed the relationships between the ultrasonic pulse velocity and the mechanical and physical properties of concrete under freeze-thaw action. The results show that the compressive strength and pulse velocity of the studied concrete changed little before the first 100 FT cycles but varied significantly after being subjected to 100 FT cycles and diminished linearly with increasing FT cycles. The dynamic elastic parameters of the concrete were inferred using pulse velocity calculations, and the dependence on FT cycles was very similar to that of ultrasonic pulse velocity. The concrete strength was strongly and positively correlated with ultrasonic pulse velocity. The linear regression model of between ultrasonic pulse velocity, kinetic coefficient, and compressive strength of concrete was also established. The damage incurred to the external coating material (XT-HPA + XT-SS and XT-HPS) was small, and the good performance of the concrete with the added inorganic coating after freeze-thaw cycles indicates good frost resistance.

1. Introduction

Concrete is currently one of the most widely used materials in civil engineering. It is composed of cement, aggregate, sand, and water. Its strength comes from the chemical reaction in which binders and water form a gel, hardening the aggregates and combining them together. Owing to the increasing use of concrete in construction projects, the durability of concrete structures has become an important research topic in the field of engineering materials and structures; thus, it is important to develop new methods for improving the concrete durability [1]. In the report that describes the progress of concrete durability studies over the span of the last 50 years, Mehta [2] pointed out that, at present, there are three main causes of concrete failure in the world: (1) steel bar corrosion, (2) freeze-thaw damage, and (3) physicochemical action owing to the presence of erosive environments.

In the northern hemisphere at mid- to high latitudes, the damage to reinforced concrete structures caused by freeze-thaw cycles has attracted much attention for the past decades [3]. In America, many reinforced concrete structures were built in extremely cold areas and the FT process critically affects the mechanical behaviour of concrete [4]. In Canada, infrastructure has been rapidly deteriorating as a result of the cold weather conditions, such as FT cycles, deicing salt, and persistent cold weather [5]. In the cold areas of China, such as on the Tibetan Plateau, in Southwest China, and in

Xinjiang, concrete structures of reinforced concrete are subjected to freezing-thawing for long periods of time, and the daytime-night temperature variations are significant, which constitutes natural conditions for freeze-thaw cycles. China spans a vast territory, seasonal permafrost covers about 53% of China's area, and permafrost accounts for ~21.5% [6], where the permafrost is mainly distributed in the low- and midlatitude regions, known as the third pole of the world on the Qinghai-Tibet Plateau; thus, freeze-thaw cycles significantly contribute to the destruction of concrete. Freeze-thaw damage of concrete is mainly assessed according to the currently applicable durability codes. The degree of damage is quantified based on indices such as mass damage, compressive strength, and relative dynamic modulus of elasticity after freeze-thaw cycles [7, 8].

The quality of a concrete structure is closely related to its mechanical and physical properties. Among the physical properties of concrete, concrete strength is generally considered to be the most important characteristic. Many techniques have been proposed for evaluating concrete strength, but those traditional nondestructive testing methods cannot provide a full and reliable concrete strength evaluation. The ultrasonic pulse velocity method is widely used for studying the physical properties of concrete [9–17], which is used for assessing concrete strength, presence and nature of defects in concrete, and the concrete thickness, by observing the propagation speed of ultrasonic impulses, reflected pulses, and shock pulses through the concrete [18]. These methods are usually based on observing the pulse propagation speed, which is closely related to the physical properties and elastic modulus of concrete.

The method of ultrasonic pulse velocity is a method of measuring concrete strength. Because of its obvious advantage as a nondestructive testing (NDT) method, the ultrasonic pulse velocity method is widely used for studying the integrity and physical properties of concrete structures [9, 15, 17]. At the same time, the ultrasonic pulse velocity technology is one of the most commonly used NDT for determining the performance of concrete.

Antonaci studied the behaviour of the existing interfaces using the nonlinear ultrasonic nondestructive testing method and revealed the effectiveness of specimens with a discontinuity surface under a compression load in describing the mechanical evolution of concrete [19]. Dynamic modulus of elasticity (DME) is an indispensable and important factor for assessing the quality and performance of concrete structures [20, 21]. Ultrasonic pulse velocity is an available parameter for estimating the Poisson ratio and dynamic modulus of elasticity (DME) [22]. Wen and Li studied the dynamic modulus of elasticity (DME) of concrete using the compressive pulse velocity method [23]. Mardani-Aghabaglou et al. evaluated the frost resistance of high-content fly fume concrete and found that dynamic modulus of elasticity (DME) corresponds to the percentage of mass change during freeze-thaw cycles [24]. Trtnik et al. analysed the parameters affecting ultrasonic pulse speed-strength relationship in concrete and analysed the relationships between ultrasonic pulse speed, static and dynamic Young's moduli, and shear modulus [25]. Lei et al. measured the thickness of the surface damage layer and the relative dynamic modulus of elasticity (RDME) of concrete using the ultrasonic pulse velocity method and effectively estimated the deterioration degree of concrete [26]. Yan predicted the service life of concrete under freeze-thaw action using ultrasonic pulse velocity [27].

NDT method of concrete with the P-pulse velocity method has been popular owing to its simplicity and low cost. Most countries have developed standardised testing procedures [28], where the concrete strength is evaluated using the pulse speed method, and a national standard is used for NDT of concrete [28]. Examples include the British 4408 standard [29]. In general, these tests nondestructively estimate the concrete strength, but other nondestructive testing methods are also used.

Considering the influence of prolonged FT cycles on the concrete project on Qinghai-Tibet Plateau, the impacts of three methods of protective inorganic coating of silica fume concrete mixed with high-permeability inorganic crystallisation water-repelling agents were studied in this work. The ultrasonic test and compressive strength test of concrete under FT cycles were conducted, and for all studied types of concrete, the dynamic elastic mechanical parameters of the concrete subjected to freeze-thaw treatment were inferred from the ultrasonic pulse velocity calculation. The mechanical properties and damage patterns of the three concrete types subjected to freeze-thaw treatment were obtained. These studies indicated inner-doped high-permeability inorganic crystalline waterproof agent silica-ash concrete with better antifreezing durability.

2. Materials Preparation and Methodology

2.1. Materials

2.1.1. Cement. Portland 42.5R cement with a specific gravity of 3.15 g/cm^3 and a specific surface area of 345 m^2/kg was used and its chemical composition is shown in Table 1.

2.1.2. Natural Aggregate. The fine aggregate is natural river sand of Tao River, with mud content less than 0.2%, and the coarse aggregate is hammer crushed stone of limestone quality, with a grain size of 5–20 mm.

2.1.3. Silica Fume (SF) and Plasticiser. Silica fume with the average particle size of 0.10 μm was used, whose chemical composition is listed in Table 2. The plasticiser of polycarboxylic acid high-efficiency water-reducing agent was used.

2.1.4. External Inorganic Coating Materials and Methods. External inorganic coating materials are as follows: (1) XT-HPA environmental protection type high-permeability inorganic crystalline waterproofing agent (permeable type): it can penetrate into the concrete interior, forming a hydrophobic coating, making the concrete hydrophobic, and stopping the erosive media such as chloride ions and sulfate ions brought in by water; (2) XT-SS environmental surface sealer (sealing type): it can form a physical barrier to protect the concrete and effectively prevent the infiltration of various chloride ions, sulfate

Table 1: Chemical composition of cement (%).

Composition	CaO	SiO_2	Fe_2O_3	Al_2O_3	SO_3	MgO	K_2O
Cement (%)	62.28	21.08	3.96	5.47	2.63	1.73	0.80

Table 2: Chemical composition of SF (%).

Composition	SiO_2	Fe_2O_3	Al_2O_3	SO_3	MgO	K_2O	CaO
Cement (%)	93.70	0.80	0.30	0.50	0.20	0.30	0.20

ions, and other aggressive media brought in by water into the concrete; (3) XT-HPS environmental protection type high-permeability enhanced sealant (composite type): it can form both a dense coating on the surface and a hydrophobic coating in the infiltrated concrete; because this coating has both a physical barrier and a hydrophobic coating of dual protection, it has an excellent effect on preventing the entry of water and its corrosive media brought in.

The spraying method of inorganic coatings applied to concrete with polypropylene fibers is as follows: concrete specimens in the water after 28 days of natural maintenance are removed from the water to clean the surface impurities and natural drying after 24 hours, the use of water-filled pneumatic spray cans will be wet concrete surface, pay attention to the surface of concrete specimens which cannot have bright water, spray the entire concrete surface once XT-HPA environmental protection type high-permeability inorganic crystalline waterproofing agent, after the surface of concrete specimens dry, spray them again (Figure 1(a)). After an interval of 24 hours, the surface of concrete specimens were cleaned with water and sprayed with XT-SS environmental surface sealer once, and after the concrete specimens were naturally dried for 24 hours, various strength tests were conducted on them (Figure 1(b)). After all strength tests were completed, the concrete specimens will continue to be tested in the FT cycles and were in a water-filled condition during the FT cycles.

2.1.5. Other Materials. Lanzhou drinking water was used. The design parameters and external coating materials of concrete are listed in Table 3.

2.2. Freeze-Thaw Testing Process of Concrete. The freeze-thaw resistance of each group of concrete was tested according to GB/T50082-2009 [30]. Three 100 mm × 100 mm × 400 mm specimens and twenty-seven standard cubic briquettes with a side length of 100 mm were prepared for each mix design. After 28 days in water, all specimens were inserted into the freeze-thaw testing machine, and the FT temperature was in the range from $-17 \pm 2^{\circ}$C to $8 \pm 2^{\circ}$C. The average RDME and mass loss rates were detected every 50 cycles up to mass loss rate arrived at 5% or three hundred cycles.

2.3. NDT Using Ultrasonic Testing

2.3.1. The Device and the Principle of Ultrasonic Testing. The ultrasonic testing device was based on an RSM-SY5 (T) type nonmetallic sound pulse detector developed by Wuhan Geotechnical Institute of the Chinese Academy of Sciences, which was composed of a wire, an acoustic detector, a receiving transducer, and a transmitting transducer. The frequency of the compressive pulse transducer is 50 kHz, and the frequency of the shear pulse transducer is 200 kHz. The sampling interval was in the 0.1–200 μs range, the recording length was in the 0.5–1 kμs range, the transmission voltage was 500 V/1000 V, the amplification gain was 100 dB, the transmission pulse width was in the 0.1–100 μs range and was continuously adjustable, and the bandwidth of the frequency band was in the 0.3–300 kHz range. To make the test results comparable, the parameters of the acoustic detector were consistent throughout the entire test process. Compared with previously used instruments, the transducer frequency of the new ultrasonic detector RSM-SY5 (T) was lower and the pulse could penetrate thicker samples. Therefore, the samples were not subjected to slicing, the disturbance of the samples was smaller, the obtained data were more accurate, and the nondestructive testing results for the concrete samples and the comparison of the test result in terms of mechanical and physical properties of the concrete samples were facilitated.

The ultrasonic detector generated repetitive electric pulses and stimulated the emission transducer. The ultrasonic pulses emitted by the transmitting transducer were coupled to the tested sample, propagated in the sample, and then detected and converted into electrical signals by the receiving transducer. The electric signals were sent to the ultrasonic instrument and the waveforms were drawn and recorded by the instrument. Ultrasonic pulse propagation time in the sample is determined by the ultrasonic pulse propagation speed. To measure ultrasonic pulse propagation time correctly, it was necessary to correct the time of the sound propagation, to identify the type of the pulses, and to determine the first pulse.

The sound propagation time was calculated according to the following formula:

$$t = t_i - t_0 - t', \tag{1}$$

where t is the time of the sound propagation after correcting the measuring point (μs), t_i is the time of the sound propagation of the P-pulse and S-pulse before correcting the measuring point (μs), t_0 is the system delay time (μs), and t' is the correction for the time of the sound propagation (μs).

Therefore, the equations for determining the velocities of the P-pulse and shear pulse were as follows, respectively:

$$V_P = \frac{L}{t_P - t_0 - t'},$$
$$V_S = \frac{L}{t_S - t_0 - t'}, \tag{2}$$

where V_P is compressive pulse velocity (km/s), V_S is shear pulse velocity (km/s), L is test-piece length (mm), t_p is the sound propagation time of compressive pulse before correcting the measuring point (μs), and t_s is the time of the sound propagation of the S-pulse before correcting the measuring point (μs).

Table 3: Concrete mix proportions.

Strength grade	Sample	Cement (kg/m^3)	Limestone (kg/m^3)	Sand (kg/m^3)	Water (kg/m^3)	Silica fume (kg/m^3)	Water-reducing agent (kg/m^3)	XT-HPA material (kg/m^3)	Water-binder ratio	External inorganic coating materials
C40	C40-A1-NCTC	418	999	785	176	22	2.2	2.2	0.4	XT-HPA + XT-SS
C40	C40-A2-NCTC	418	999	785	176	22	2.2	2.2	0.4	None
C40	C40-A3-NCTC	418	999	785	176	22	2.2	2.2	0.4	XT-HPS

Figure 1: Inorganic coating spraying of concrete. (a) Concrete samples and coating material; (b) concrete surface morphology after inorganic coating spraying.

2.3.2. Ultrasonic Testing Method. The propagation speed of ultrasonic pulses in the studied concrete samples was measured using an RSM-SY5 (T) nonmetallic acoustic detector, as shown in Figure 2. Because the attenuation of concrete is greater than that of other nonmetallic materials, the frequencies were in the 20–100 kHz range. The test procedure was as follows:

(1) Vaseline was used as a coupling medium to ensure good contact between concrete and sensors.

(2) The instrument parameters were set as follows. For the ultrasonic P-pulse velocity test, the sampling interval was 1 μs, the sampling length was 512 μs, the transmitted pulse width was 50 μs, and the emission voltage was low. For the ultrasonic S-pulse velocity test, the sampling interval was 0.5 μs, the sampling length was 512 μs, the transmitted pulse width was 50 μs, and the emission voltage was low. The calibration values of the instruments were set, respectively.

(3) When sampling, the transmitting transducer and the receiving transducer were pressed and stored when the waveform was stable, so that shear pulse velocity and compressive pulse velocity of concrete specimens with different mix ratios could be measured.

2.4. Compressive Strength Test. Cubic briquettes with 100 mm side lengths were used for concrete compressive strength testing, and there were three briquettes in each group. The test was conducted using a 2000-kN electrohydraulic servo-pressure testing machine (Figure 3); a detailed description can be found in "Standard of Test Methods for Mechanical Properties of Ordinary Concrete (GB/T50081-2002)" [31]. The loading speed was 0.20 MPa/s to the failure.

After 50 freeze-thaw cycles, a set of concrete briquettes was taken for measuring the compressive strength, and its average value (over the briquettes) was calculated.

3. Results and Discussion

3.1. Characteristics of Variation of Ultrasonic Pulse Velocity of Concrete during FT Cycles

3.1.1. The Decay Rate of Ultrasonic Compressive Pulse Velocity. We used the ultrasonic detector RSM-SY5 (T) to measure the ultrasonic compressive pulse velocity of the concrete specimens for different numbers of FT cycles, for calculating the decay of the compressive pulse velocity.

After every 50 FT cycles, the surface moisture was wiped from the tested concrete specimens, and ultrasonic compressive pulse velocity was measured according to the above-described method. Equation (3) was used for calculating the decay rate of the compressive pulse velocity of the concrete samples:

$$P_v = \frac{V_{P_0} - V_{P_n}}{V_{P_0}} \times 100\%, \quad (3)$$

where P_v is the decay rate of compressive pulse velocity of concrete, V_{P_n} is the velocity of the compressive pulse after FT cycles (km/s), and V_{P_0} is the velocity of the compressive pulse before freeze-thaw cycles (km/s).

Figure 4 shows the variation of the compressive pulse velocity and its decay rate during 300 FT cycles for the tested concrete samples coated using three different methods as described above. As can be seen from Figure 4(a), the trends of the compressive pulse velocity for the three groups of tested concrete specimens (C40-A1-NCTC, C40-A2-NCTC, and C40-A3-NCTC (number of three groups of concrete mix ratio)) subjected to FT cycles were similar. In general,

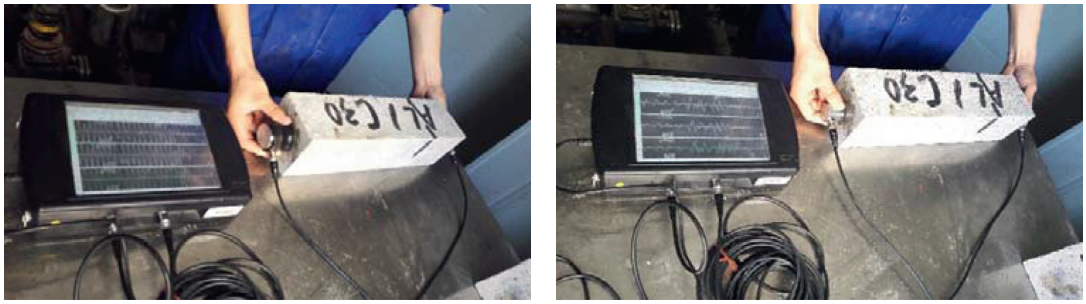

(a) (b)

Figure 2: Photograph of ultrasonic velocity tests. (a) Ultrasonic compressive pulse velocity test; (b) ultrasonic shear pulse velocity test.

Figure 3: MATEST digital display pressure tester.

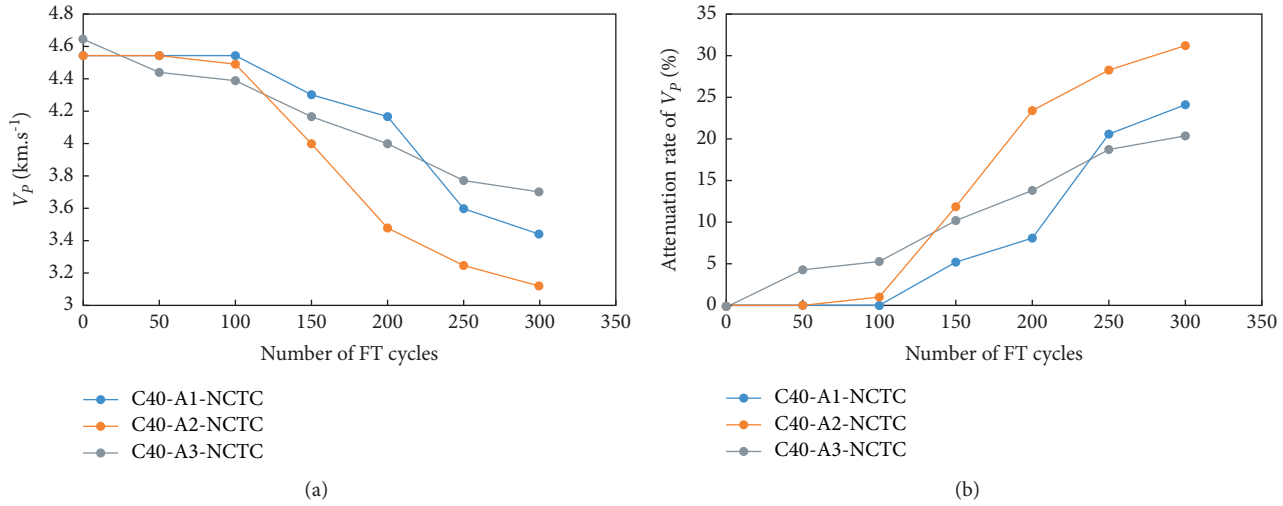

(a) (b)

Figure 4: Variation characteristic of ultrasonic compressive pulse velocity and its decay rate of three kinds of concrete over 300 FT cycles. (a) Variation characteristic of ultrasonic compressive pulse velocity; (b) decay rate of ultrasonic compressive pulse velocity.

the compressive pulse velocity tended to decrease; the rate of attenuation was relatively slow during the first 100 FT cycles but then increased rapidly. The compressive pulse velocity and the attenuation rate during the FT cycles are shown in Figure 4(b) and Table 4.

From Figure 4(b) and Table 4, the initial P-pulse velocities for the three types of tested concrete samples are similar for no FT cycles, but the decay rates become different after 300 FT cycles. The concrete sample sprayed with the XT-HPA inorganic coating and the XT-SS inorganic coating (C40-A1-NCTC) and concrete specimens sprayed with the XT-HPA inorganic coating (C40-A3-NCTC) exhibit smaller ultrasonic pulse velocity decay than unsprayed inorganic coated concrete specimens (C40-A2-NCTC), whose specific parameters are listed in Table 5.

The compressive pulse velocities for the three kinds of concrete specimens were close to those of the three groups of concrete samples before the FT treatment. Nevertheless, after 300 FT cycles, the compressive pulse velocities for group A (C40-A1-NCTC to C40-A3-NCTC) were 3.45 km/s, 3.13 km/s,

Table 4: Parameters of linear relationship between ultrasonic compressive pulse velocity and shear pulse velocity.

Specimen	a	b	Determination coefficient
All samples	0.6102	0.0713	0.9936
C40-A1-NCTC	0.6044	0.0977	0.9984
C40-A2-NCTC	0.6108	0.0692	0.9993
C40-A3-NCTC	0.6182	0.036	0.9679

Table 5: Variation characteristic in the ultrasonic compressive pulse velocity of three kinds of concrete under FT cycles.

Specimen	V_P at 0 FT cycles (km/s)	V_P at 300 FT cycles (km/s)	Decay rate of V_P (%)
C40-A1-NCTC	4.55	3.45	24.14
C40-A2-NCTC	4.55	3.13	31.24
C40-A3-NCTC	4.65	3.70	20.36

and 3.70 km/s, respectively. The decay rates of the compressive pulse velocities were 24.14%, 31.24%, and 20.36%, respectively, which was very different from the values for the other spraying methods. These results show that the external inorganic coating of concrete improves the antifreezing performance.

3.1.2. The Decay Rate of Ultrasonic Shear Pulse Velocity. The ultrasonic detector RSM-SY5 (T) was used for measuring the ultrasonic shear pulse velocity of the tested concrete specimens, for different numbers of FT cycles.

After every 50 FT cycles, the surface moisture was wiped from the tested concrete samples, and the ultrasonic shear pulse velocity was measured according to the above-described test method. Equation (4) was used for calculating the attenuation rate of shear pulse velocity of concrete specimens:

$$S_v = \frac{V_{S_0} - V_{S_n}}{V_{S_0}} \times 100\%, \tag{4}$$

where S_v is the decay rate of shear pulse velocity of a concrete specimen, V_{S_n} is shear pulse velocity after an FT cycle (km/s), and V_{S_0} is shear pulse velocity before the freeze-thaw cycle (km/s).

Figure 5 shows the variation of the shear pulse velocity and its attenuation rate during 300 FT cycles, to concrete specimens coated using three different methods. According to Figure 5(a), shear pulse velocity variations during the FT cycles are similar for three types of concrete (C40-A1-NCTC to C40-A3-NCTC) and all exhibit decreasing trends. The pulse velocity decay is slow in the first 100 FT cycles but decays rapidly after the first 100 FT cycles. Shear pulse velocities and decay rates during freeze-thaw cycles are shown in Figure 5(b) and Table 6.

From Figure 5(b) and Table 6, the initial shear pulse velocities of concrete with inorganic coatings are similar when no FT cycles are applied. After 300 FT cycles, the attenuation patterns of shear pulse velocity for three kinds of concrete become distinctly different. The concrete specimen sprayed with the XT-HPA inorganic coating and XT-SS inorganic coating with surface sealant (C40-A1-NCTC) and concrete specimen sprayed with the XT-HPA inorganic coating (C40-A3-NCTC) exhibit smaller shear pulse velocity decay than unsprayed inorganic concrete specimen (C40-A2-NCTC) with inorganic coating, whose specific parameters are listed in Table 6.

The variation of shear pulse velocities for three kinds of concrete is similar to that of compressive pulse velocities. The values are close for three kinds of concrete before FT treatment; however, after 300 FT cycles, shear pulse velocities for three types of concrete (C40-A1-NCTC to C40-A3-NCTC) are 2.18 km/s, 1.97 km/s, and 2.31 km/s, respectively, and the decay rates of shear pulse velocities are 23.33%, 30.49%, and 19.29%, respectively, which is very different from the values for other spraying methods. These results show that the external coating of inorganic coating improves the frost resistance of concrete.

3.2. Variation of the Kinetic Coefficient of Concrete during Freeze-Thaw Cycles

3.2.1. The Standard Method of Kinetic Parameters. The dynamic elastic modulus E, the dynamic shear modulus G, and the Poisson ratio μ of concrete define its basic mechanical properties. At present, the methods for quantifying these three dynamic parameters mainly include the resonance column method, the pulse velocity method, and the dynamic three (single) test method. Compared with other methods, the pulse velocity method is simple, nondestructive, and fast; as a result, it is widely used for nondestructive testing of concrete. However, the existing pulse velocity method is mainly used for simple determination of the pulse velocity, but the dynamic elastic modulus, the dynamic shear modulus, and the pulse velocity ratio of concrete are less commonly quantified using the pulse velocity method. Based on the elastic theory, the measured P-pulse velocity V_P, the shear pulse velocity V_S, and the sample density ρ are used for determining these quantities of interest. The equations for computing the above three quantities are as follows:

$$E = \frac{\rho V_S^2 \left(3V_P^2 - 4V_S^2\right)}{V_P^2 - V_S^2}, \tag{5}$$

$$G = \rho V_S^2, \tag{6}$$

$$\mu = \frac{V_P^2 - 2V_S^2}{2\left(V_P^2 - V_S^2\right)}, \tag{7}$$

where ρ is the tested sample's density (g/cm^3).

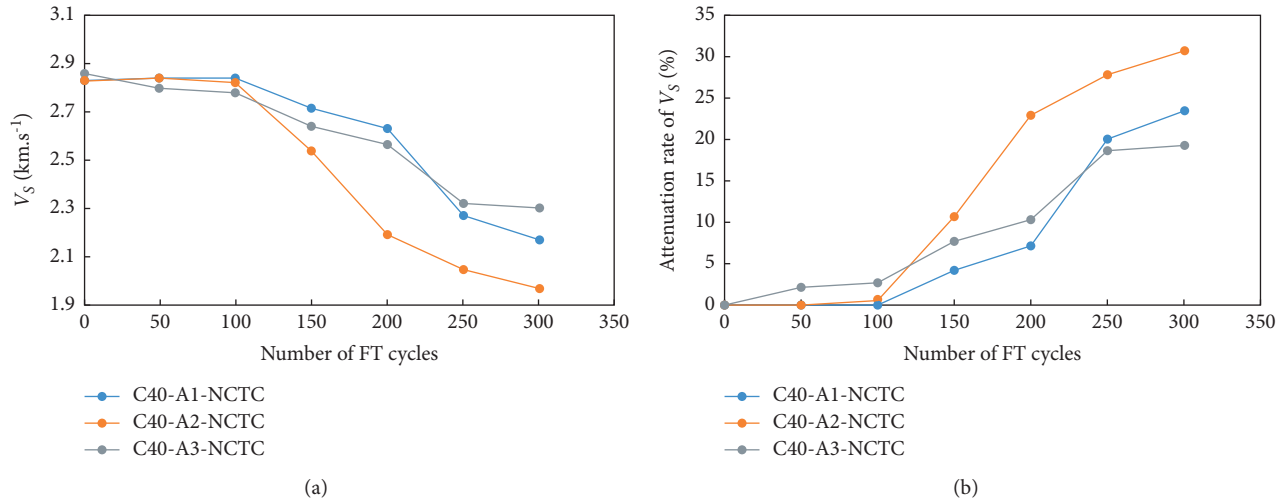

Figure 5: Variation characteristic of ultrasonic shear pulse velocity and its decay rate of three kinds of concrete over 300 FT cycles. (a) Variation characteristic of ultrasonic shear pulse velocity; (b) decay rate of ultrasonic shear pulse velocity.

Table 6: Variation characteristic in the ultrasonic shear pulse velocity of three kinds of concrete under FT cycles.

Specimen	V_S at 0 FT cycles (km/s)	V_S at 300 FT cycles (km/s)	Decay rate of V_S (%)
C40-A1-NCTC	2.84	2.18	23.33
C40-A2-NCTC	2.84	1.97	30.49
C40-A3-NCTC	2.86	2.31	19.29

The relationships between dynamic modulus of elasticity (DME) E, dynamic shear modulus (DSM) G, Poisson's ratio μ, and the number of FT cycles are shown in Figure 6. From Figure 6, the variation trends of DME E and DSM G of concrete with FT cycles are similar to ultrasonic pulse velocity under FT cycles; these quantities decrease with increasing FT cycles, and these trends become very clear after 100 FT cycles.

Figures 6(a) and 6(b) show the variation characteristics of DME and DSM, computed using ultrasonic pulse velocity method (equations (5) and (6)), for the three kinds of concrete specimens, during 300 FT cycles. Figure 6(c) shows the changes in the Poisson ratio for the three types of concrete specimens, during 300 FT cycles.

From Figure 6(a), DME for three types of concrete decrease relatively slowly during the first 100 freeze-thaw cycles, but the rate of attenuation increases after the first 100 freeze-thaw cycles. After 300 FT cycles, DME for three types of concrete (C40-A1-NCTC to C40-A3-NCTC) are 27.262 GPa, 22.458 GPa, and 31.541 GPa. Relative dynamic moduli of elasticity (RDME) are 57.81%, 46.22%, and 64.37%, respectively, which shows that both of the three concrete types reached the failure criterion; overall, the two types of concrete demonstrate poor antifreezing.

From Figures 6(a) and 6(b), variation characteristics of DME and DSM of concrete types during FT treatment are similar. The dynamic shear moduli for three kinds of concrete (C40-A1-NCTC to C40-A3-NCTC) decrease relatively slowly during the first 100 FT cycles, but the rate of attenuation is much higher after the first 100 FT cycles. After 300 FT cycles, the dynamic shear moduli for three concrete types (C40-A1-NCTC to C40-A3-NCTC) are 11.66 GPa, 9.61 GPa, and 13.32 GPa, respectively. The respective relative dynamic shear moduli are 59.18%, 48.18%, and 66.18%.

For three kinds of concrete, the Poisson ratio during FT treatment gradually decreases (Figure 6(c)).

3.2.2. Damage Amount. The damage amount D can describe the damage and performance degradation of concrete [32, 33], and the following equation is obtained using the dynamic elastic modulus concept:

$$D = \frac{E_0 - E_t}{E_0}, \tag{8}$$

where E_0 is initial DME (GPa) and E_t is DME after FT treatment (GPa).

Figure 7 shows the relationship between the number of FT cycles and the damage amount, for the three types of concrete. From Figure 7, the relationship between the number of FT cycles and the amount of damage to the concrete differs depending on the type of concrete coating. During the first 100 FT cycles, the damage amount for the three types of concrete is small, and the amount of damage actually decreases for two of three kinds (C40-A1-NCTC and C40-A2-NCTC), which suggests that a small number of FT cycles can increase the strength of concrete. Beyond 100 FT cycles, the damage amount for the three groups of samples increases rapidly, and the damage amount for C40-A2-NCTC is the greatest.

After 300 FT cycles, the damage amount for three kinds of concrete samples is as follows: C40-A1-NCTC < C40-A3-NCTC < C40-A2-NCTC.

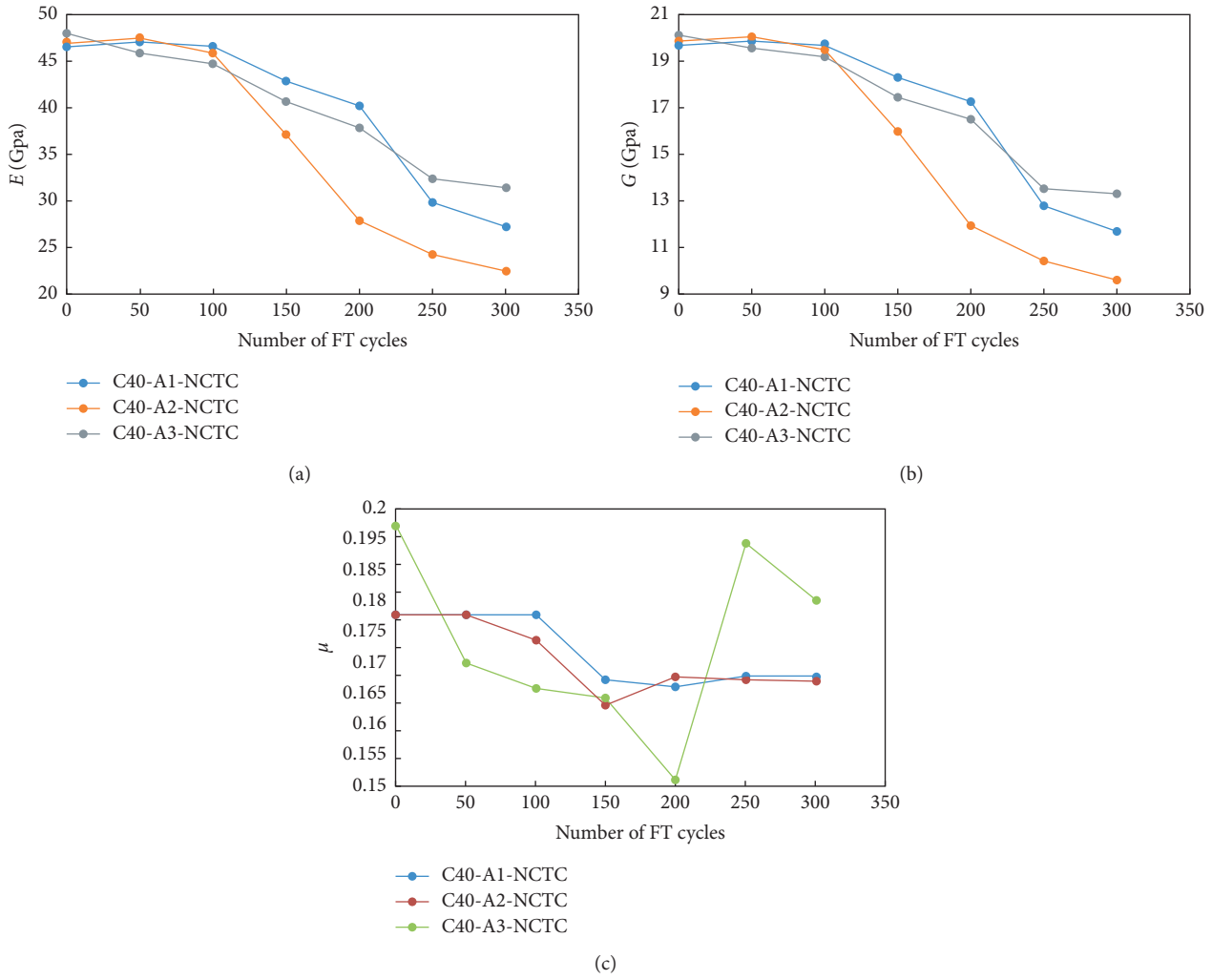

Figure 6: Variation characteristic of DME, DSM, and Poisson's ratio of three kinds of concrete over 300 FT cycles. (a) Variation characteristic of DME; (b) variation characteristic of DSM; (c) variation characteristic of Poisson's ratio.

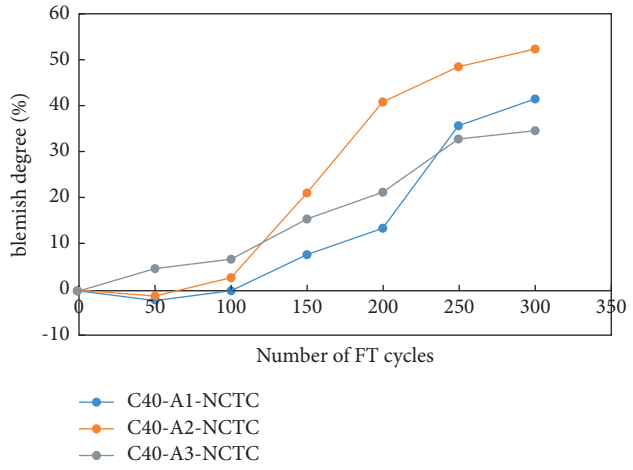

Figure 7: The relationship curve between the damage amount of three kinds of concrete and the number of FT cycles.

3.3. Mass Loss of Concrete with External Inorganic Coating during FT Treatment. Figure 8 indicates variation characteristics of mass loss for concrete subjected to the freeze-thaw treatment. From Figure 8, during the first 100 FT cycles, the mass loss of concrete is small. Nevertheless, after the first 100 FT cycles, loss rate of mass becomes much smaller, with mass loss rates for the three types of concrete being 1.73% (for C40-A1-NCTC), 1.47% (for C40-A2-NCTC), and 0.44% (for C40-A3-NCTC). The trends of the mass loss and the damage amount were similar for the three types of concrete. However, the failure standard of GB/T 50082-2009 has not been met for the mass loss [30], which suggests that coating enhances the bonding properties of concrete to a certain extent, helping to reduce its mass loss.

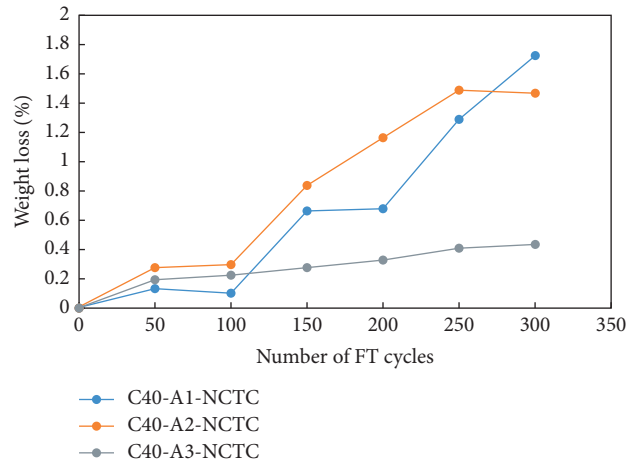

Figure 8: Weight loss of three kinds of concrete specimens under FT cycles.

3.4. Loss Rate of Compressive Strength. According to GB/T 50082-2009 [30], the compressive strength per 50 FT cycles was tested for three kinds of concrete. The formula for calculating the loss rate p of the concrete compressive strength was

$$p = \frac{f_0 - f}{f_0} \times 100\%, \tag{9}$$

where p is the loss rate of the compressive strength of concrete, f is the compressive strength of concrete after the freeze-thaw treatment (MPa), and f_0 is the initial compressive strength of concrete without the freeze-thaw treatment (MPa).

Figures 9 (a) and 9(b) show variations in the compressive strength and the loss rate of the compressive strength for three kinds of concrete subjected to FT treatment. These figures show that, for the three types of concrete subjected to the freeze-thaw treatment, the loss rate of the compressive strength of concrete is similar to that of damage amount and attenuation rate of ultrasonic pulse velocity, which shows that the loss rate of the compressive strength of concrete increases linearly with increasing the number of freeze-thaw cycles. The loss rates of the compressive strengths for the two types of concrete (C40-A1-NCTC and C40-A2-NCTC) decrease somewhat during the first 150 FT cycles and then increase sharply. After 300 FT cycles, the compressive strengths for the three types of concrete (C40-A1-NCTC to C40-A3-NCTC) were 52.37 MPa, 50.00 MPa, and 54.24 MPa, respectively. The respective loss rates of the compressive strength were 21.66%, 25.02%, and 19.11%.

Figure 9(c) shows an example image of concrete failure following the compressive strength test after 300 FT cycles, which shows good cementing performance.

After 300 FT cycles, the relative dynamic moduli of elasticity for two of the three concrete types are below 60%, which meets the national standard of failure, for which the loss rate of the concrete compressive strength should be above 19.00%. However, the compressive strength was still above 50.00 MPa, which is much higher than the national standard for C40 concrete. This observation shows that concrete with inorganic coating has good frost resistance, and it also suggests that there are some limitations on the standard of the relative dynamic elastic moduli under 60%.

3.5. Relationship between the Ultrasonic Shear Pulse Velocity, Dynamic Coefficient, Compressive Strength, and Ultrasonic Compressive Pulse Velocity for Concrete Subjected to the Freeze-Thaw Treatment. The relationships between the ultrasonic shear pulse velocities, the dynamic coefficients, the compressive strengths, and the ultrasonic compressive pulse velocities for the three kinds of concrete subjected to FT treatment were gained using the linear regression analysis. The relationships were modelled as follows:

$$\begin{aligned} V_S &= aV_P + b, \\ E &= a'V_P + b', \\ G &= AV_P + B, \\ f &= A'V_P + B', \end{aligned} \tag{10}$$

where a, b, a', b', A, B, A', and B' are correlation coefficients, which are related to the mixing proportions of concrete materials. In this test, the values of the concrete correlation coefficients (a, b, a', b', A, B, A', and B') for three kinds of concrete subjected to FT treatment are listed in Tables 4, 7–9, respectively.

The results in Tables 4 and 7–9 show that the linear regression model linking ultrasonic pulse velocity, dynamic coefficient, compressive strength, and ultrasonic pulse velocity of concrete yields the determination coefficient above 0.90. This suggests a good correlation between the ultrasonic pulse velocity and the dynamic elastic modulus and provides the basis for further studies on the relationship between the strength of concrete estimated using the ultrasonic method and FT cycles.

Figure 10(a) shows the ratio of ultrasonic shear pulse velocity V_S to compressive pulse velocity V_P, for 21 concrete specimens subjected to FT treatment. The ratio of ultrasonic shear pulse velocity V_S to compressive pulse velocity V_P for concrete subjected to FT treatment is mainly distributed between 0.61 and 0.63.

Figure 10(b) shows the ratio of dynamic shear modulus G to dynamic elastic modulus E, for 21 concrete samples subjected to the FT treatment. The ratio of dynamic shear

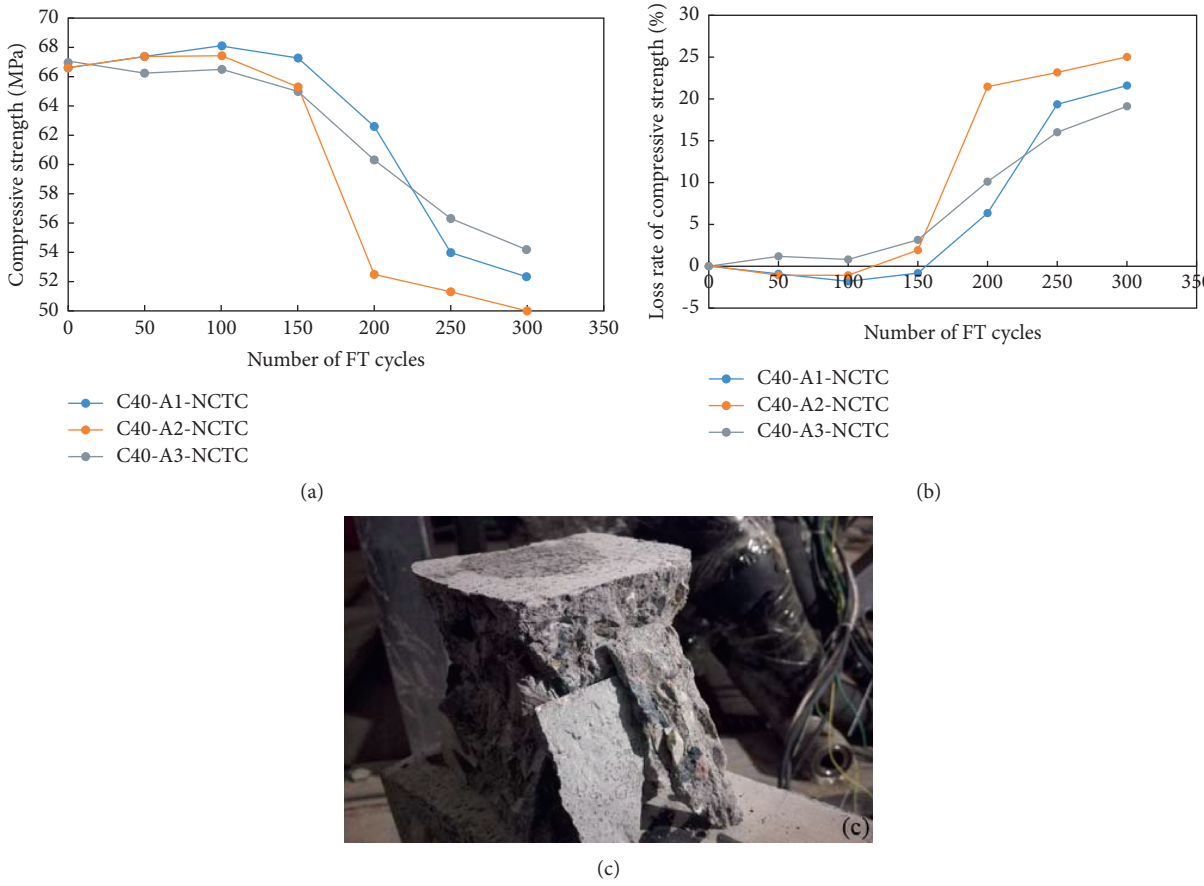

Figure 9: Variation curve of compressive strength and the loss rate of compressive strength of three kinds of concrete during FT cycles. (a) Variation characteristics of compressive strength; (b) loss rate of compressive strength; (c) failure image of concrete after compressive strength test.

Table 7: Parameters of linear relationship between ultrasonic compressive pulse velocity and dynamic modulus of elasticity.

Specimen	a'	b'	Determination coefficient
All samples	17.775	−33.762	0.9969
C40-A1-NCTC	17.913	−34.501	0.9988
C40-A2-NCTC	17.594	−32.909	0.9991
C40-A3-NCTC	18.435	−36.495	0.9894

Table 8: Parameters of linear relationship between ultrasonic compressive pulse velocity and dynamic shear modulus.

Specimen	A	B	Determination coefficient
All samples	7.4618	−13.95	0.9924
C40-A1-NCTC	7.4878	−14.118	0.9975
C40-A2-NCTC	7.3929	−13.626	0.9994
C40-A3-NCTC	7.7563	−15.169	0.9656

Table 9: Parameters of linear relationship between ultrasonic compressive pulse velocity and compressive strength.

Specimen	A'	B'	Determination coefficient
All samples	13.269	7.515	0.9359
C40-A1-NCTC	14.361	2.8576	0.9636
C40-A2-NCTC	12.814	9.8827	0.9408
C40-A3-NCTC	14.169	3.2907	0.9084

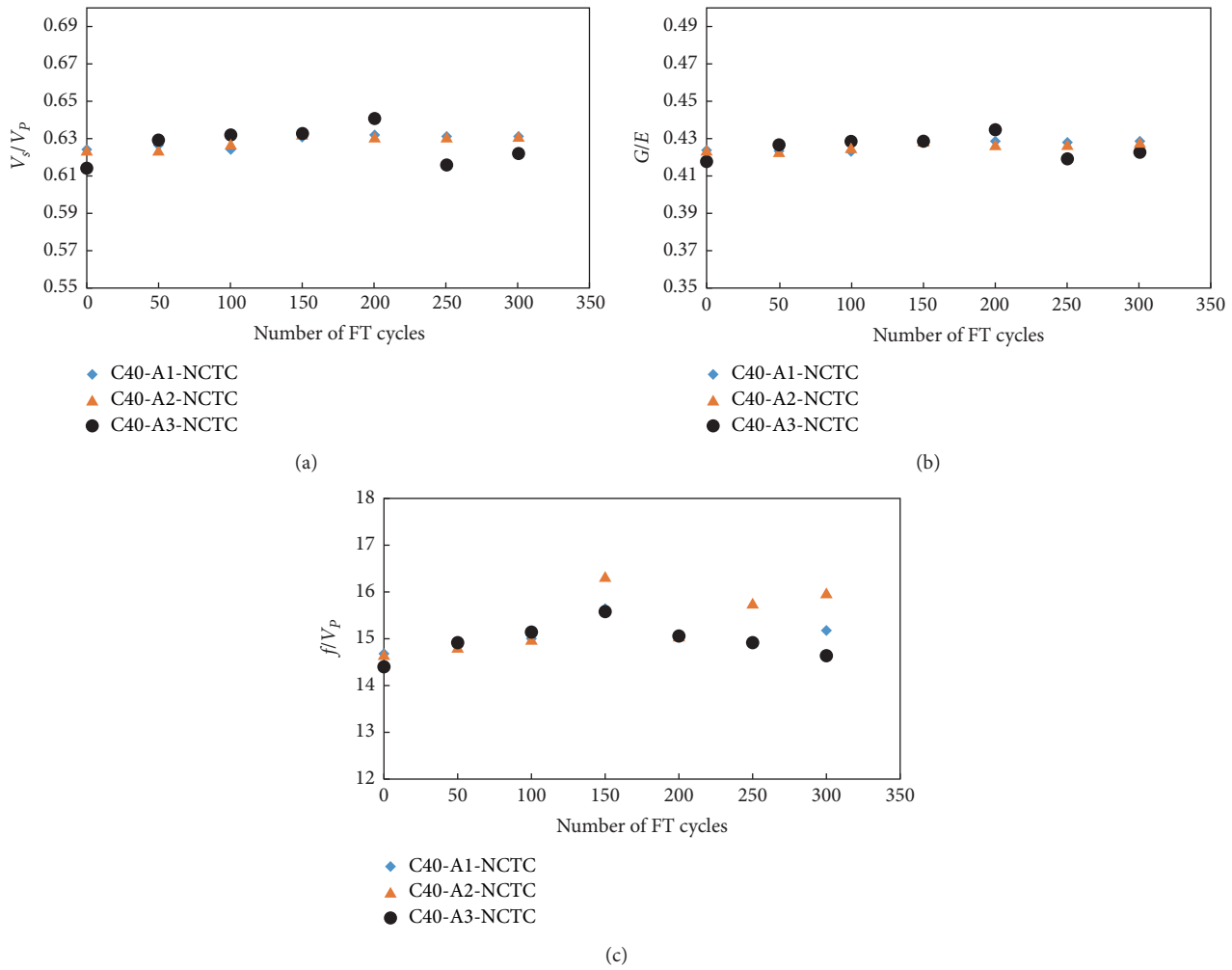

Figure 10: The ratio of dynamic strength to compressive pulse velocity of concrete under FT cycles. (a) V_S/V_P; (b) G/E; (c) f/V_P.

modulus G to dynamic elastic modulus E for concrete subjected to the freeze-thaw treatment is mainly distributed between 0.42 and 0.43.

Figure 10(c) shows the ratio of concrete compressive strength f to compressive pulse velocity V_P, for 21 concrete samples subjected to FT treatment. The ratio of the compressive strength f to the compressive pulse velocity V_P for concrete subjected to FT treatment is mainly distributed between 14.6 and 16.0. There is significant discreteness, which indicates that individual briquette characteristics significantly affect the compressive strength, but there is still a good correlation between the concrete compressive strength and its compressive pulse velocity.

3.6. Strength Attenuation Mechanisation of Concrete under FT Cycles. Frost damage is due to several pore pressures caused by ice formation, that is, hydraulic pore pressure due to ice volume expansion and crystallisation and low-temperature water absorption pressure due to thermodynamic equilibrium between ice crystals and thawing water. It has also been observed that only highly saturated concrete can be damaged by frost. It can be found that the strength of concrete attenuates with the increase of freeze-thaw times, especially after 100 FT cycles. Because the freeze-thaw cycle adversely affects the strength of concrete decreasing with the increase of freeze-thaw cycles, the ultrasonic pulse velocity and compressive pulse velocity of concrete decrease with the increase of the number of freeze-thaw cycles. As for the slow attenuation of strength before 100 FT cycles, it should be that the concrete is still hydrated in the early freeze-thaw cycle, so the strength also increases. However, after 100 hydration reactions, freezing and thawing lead to a rapid decrease in strength.

4. Conclusions

In this study, the rapid freeze-thaw cycle test of internal coating silicon fume concrete with different external coatings was carried out, the strength evolution law of concrete with different external inorganic coatings was analysed by ultrasonic testing and compressive strength, and the correlation between ultrasonic pulse velocity and physical mechanics was analysed. The following conclusions were obtained in this study through theoretical derivation and experimental examinations:

(1) The compressive strength and ultrasonic pulse velocity of the studied concrete samples decreased gradually with increasing the number of freeze-thaw cycles, especially after the first 100 FT cycles. As for the slow attenuation of strength before 100 FT cycles, it should be that the concrete is still hydrated in the early FT cycle, so the strength also increases. But after 100 hydration reactions, freezing and thawing lead to a rapid decrease in strength.

(2) The trends for dynamic elastic modulus E and dynamic shear modulus G versus the number of FT cycles were similar to that of ultrasonic pulse velocity. Both moduli decreased with increasing FT cycles and also decreased dramatically after the first 100 FT cycles. For the three types of concrete, the Poisson ratios gradually decreased with increasing FT cycles.

(3) The amount of damage to the three types of concrete samples was small during the first 100 FT cycles, but after the first 100 FT cycles, the amount of damage increased rapidly. The amount of damage to the concrete samples without external coating increased sharply after the first 100 FT cycles. The damage amount to the external coating material (XT-HPA plus XT-SS and XT-HPS) of concrete was small, and the performance of the concrete samples after the freeze-thaw treatment was good, which shows good frost resistance durability. After 300 FT cycles, the damage amount for three kinds of concrete was as follows: C40-A1-NCTC < C40-A3-NCTC < C40-A2-NCTC. The respective relative dynamic elastic moduli (C40-A1-NCTC, C40-A2-5NCTC, and C40-A1-NCTC) are 57.81%, 46.22%, and 64.37%, which shows that two of the three concrete types reached the failure criterion; overall, the two types of concrete demonstrate poor antifreezing.

(4) Following the freeze-thaw treatment, the ratio of the pulse velocity V_S to the P-pulse velocity V_P of the concrete samples was mainly between 0.61 and 0.63. The ratio of the dynamic shear modulus G to the dynamic elastic modulus E was mainly distributed between 0.42 and 0.43. The ratio of the compressive strength f to the P-pulse velocity V_P of concrete subjected to the freeze-thaw treatment was mainly distributed between 14.6 and 16.0. There was a good correlation between these quantities.

(5) The relationship between ultrasonic pulse velocity and intensity of concrete was well-described by a linear function, and the coefficient of determination of the linear regression fit was above 0.90, indicating a good correlation between the ultrasonic pulse velocity and concrete intensity. Thus, the strength of concrete can be estimated by measuring its ultrasonic pulse velocity.

Data Availability

The underlying data supporting the results of this study are included within this article.

Conflicts of Interest

The authors declare that they have no conflicts of interest.

Acknowledgments

The financial support for this project was provided by the the Second Tibetan Plateau Scientific Expedition and Research Program (STEP) (Grant no. 2019QZKK0905), Scientific Research Fund of the Institute of Engineering Mechanics, China Earthquake Administration (Grant no. 2020 EEEVL0304), the Scientific Research Fund of Institute of Earthquake Forecasting, China Earthquake Administration (Grant no. 2014IESLZ01), the National Natural Science Foundation of China (Grant nos. 51678545, 41472297, and U1939209), and Topics of Gansu Province Key R&D Program (Grant no. 18YF1FA101).

References

[1] D. Gui-Zhen and F. Cong-Qi, "Research progress and new thinking of destruction of concrete due to freeze-thaw cycles," *Concrete*, vol. 12, no. 5, pp. 16–20, 2013, in Chinese.

[2] P. K. Mehta, "Concrete durability-fifty year's progress," in *Proceedings of the 2nd International Conference on Concrete Durability, ACI*, pp. 11–31, Montreal , Canada, August 1991.

[3] R. Terje Finnerup, "Freeze-thaw resistance of concrete effect of curing conditions, moisture exchange and materials," PhD dissertation, Trondheim: Norwegian Institute of Technology, Trondheim, Norway, 2001.

[4] Y. Frank, "Damage assessment, characterization, and modeling for enhanced design of concrete bridge decks in cold regions," PhD dissertation, Department of Civil and Environmental Engineering, North Dakota State University, Fargo, ND, USA, 2015.

[5] G. Mark, J. S. Dent Aaron, and A. Bisby Luke, "Effect of freeze-thaw cycling on the behavior of reinforced concrete beams strengthened in flexure with fiber reinforced polymer sheets," *Canadian Journal of Civil Engineering*, vol. 30, no. 6, pp. 1081–1088, 2011.

[6] Y. Zhou, "Frozen Soil in China," Science Publishing House, New York City, NY, USA, 2000.

[7] X. X. Wang, X. D. Shen, H. L. Wang, and C. Gao, "Nuclear magnetic resonance analysis of concrete-lined channel freeze-thaw damage," *Ceramic Society of Japan*, vol. 123, pp. 43–51, 2015.

[8] X. Wang, Y. Wu, X. Shen, H. Wang, S. Liu, and C. Yan, "An experimental study of a freeze-thaw damage model of natural pumice concrete," *Powder Technology*, vol. 339, pp. 651–658, 2018.

[9] R. S. Ravindrarajah, "Strength evaluation of high-strength concrete by ultrasonic pulse velocity method," *NDT & E International*, vol. 30, no. 4, pp. 262–275, 1997.

[10] A. Galan, "Estimate of concrete strength by ultrasonic pulse velocity and damping constant," *ACI Journals*, vol. 64, no. 10, pp. 678–684, 1967.

[11] R. Solís-Carcaño and E. I. Moreno, "Evaluation of concrete made with crushed limestone aggregate based on ultrasonic pulse velocity," *Construction and Building Materials*, vol. 22, no. 6, pp. 1225–1231, 2008.

[12] ACI 228.2R-98. Nondestructive test methods of evaluation of concrete in structures. ACI Committee 228.

[13] M. Sansalone and W. B. Streett, *Impact-echo Nondestructive Evaluation of Concrete and Masonry*, Bullbrier Press, Ithaca, NY, USA, 1997.

[14] W. F. Price and J. P. Haynes, "In situ strength testing of high strength concrete," *Magazine of Concrete Research*, vol. 48, no. 176, pp. 189–197, 1997.

[15] S. Nazarian, M. Baker, and K. Crain, "Assessing quality of concrete with wave propagation techniques," *ACI Materials Journal*, vol. 94, no. 35, pp. 296–305, 1997.

[16] Y. Wu-Jian, N. Fu-Jun, W. Zhi-Jian, N. Fuhang, L. Zhanju, and N. Zuojun, "Mechanical property of polypropylene fiber reinforced concrete under freezing-thawing cycle effect," *Journal of Traffic and Transportation Engineering*, vol. 16, no. 4, pp. 37–44, 2016.

[17] P. Turgut, "Research into the correlation between concrete strength and UPV values," *Non-Destructive Testing*, vol. 12, no. 12, pp. 56–63, 2004.

[18] A. Iwatake, "Nondestructive testing on concrete pavements by ultrasonic wave," in *Proceedings of the 3rd International Conference on NDT*, Tokyo, Japan, 1960.

[19] P. Antonaci, C. L. E. Bruno, P. G. Bocca, M. Scalerandi, and A. S. Gliozzi, "Nonlinear ultrasonic evaluation of load effects on discontinuities in concrete," *Cement and Concrete Research*, vol. 40, no. 2, pp. 340–346, 2010.

[20] A. Kar, U. B. Halabe, I. Ray, and A. Unnikrishnan, "Non-destructive characterizations of alkali activated fly ash and/or slag concrete," *European Scientific Journal*, vol. 9, no. 24, pp. 187–195, 2013.

[21] G. Singh and R. Siddique, "Effect of waste foundry sand (WFS) as partial replacement of sand on the strength, ultrasonic pulse velocity and permeability of concrete," *Construction and Building Materials*, vol. 26, no. 1, pp. 416–422, 2012.

[22] L. Qixian and J. H. Bungey, "Using compression wave ultrasonic transducers to measure the velocity of surface waves and hence determine dynamic modulus of elasticity for concrete," *Construction and Building Materials*, vol. 10, no. 4, pp. 237–242, 1996.

[23] S.-Y. Wen and X.-B. Li, "Experimental study on Young's modulus of concrete," *Journal of Central South University of Technology*, vol. 7, no. 1, pp. 43–45, 2000.

[24] A. Mardani-Aghabaglou, Ö. Andiç-Çakir, and K. Ramyar, "Freeze-thaw resistance and transport properties of high-volume fly ash roller compacted concrete designed by maximum density method," *Cement and Concrete Composites*, vol. 37, pp. 259–266, 2013.

[25] G. Trtnik, F. Kavčič, and G. Turk, "Prediction of concrete strength using ultrasonic pulse velocity and artificial neural networks," *Ultrasonics*, vol. 49, no. 1, pp. 53–60, 2009.

[26] J. Lei, N. Di-Tao, S. Ying-Zhao, and F. Qian-Nan, "Ultrasonic testing and microscopic analysis on concrete under sulfate attack and cyclic environment," *Journal of Central South University*, vol. 21, pp. 4723–4731, 2014.

[27] W. Yan, Z. Wu, F. Niu, T. Wan, and H. Zheng, "Study on the service life prediction of freeze–thaw damaged concrete with high permeability and inorganic crystal waterproof agent additions based on ultrasonic velocity," *Construction and Building Materials*, vol. 259, pp. 1–13, 2020.

[28] K. Komlos, S. Popovics, T. Nu¨rnbergerova´, B. Babál, and J. Popovics, "Ultrasonic pulse velocity test of concrete properties as specified in national standards," *Cement and Concrete Composites*, vol. 18, pp. 357–364, 1996.

[29] BS 4408, *Non-destructive Methods of Test for Concrete Measurement of the Ultrasonic Pulses Velocity in Concrete*, British Standard Institute, London, UK, 1970.

[30] Ministry of Housing and Urban-Rural Development of the People's Republic of China, GB/T 50082–2009, *Standard for Test Methods of Long-Term Performance and Durability of Ordinary Concrete*, China Construction Industry Press, Beijing, China, 2009, in Chinese.

[31] Ministry of Housing and Urban-Rural Development of the People's Republic of China, GB/T 50081–2002, *Standard of Test Methods for Mechanical Properties of Ordinary Concrete*, China Construction Industry Press, Beijing, China, 2002, in Chinese.

[32] Z. Lixiang, W. Shichao, and Z. Zaodong, "Analysis of reliability confidence limits of fatigue damage strength of concrete," *Engineering Mechanics*, vol. 21, no. 4, pp. 139–143, 2004, in Chinese.

[33] Y. Tianqing and Q. Jicheng, *The Theory and Application of Blemish*, National Defense Industry Press, Beijing, China, 1991, in Chinese.